INTERPRETATION OF PAINTER STREET OVERCROSSING RECORDS TO DEFINE INPUT MOTIONS TO THE BRIDGE SUPERSTRUCTURE

K. Romstad
Professor of Civil Engineering, University of California, Davis

B. Maroney
Graduate Student, University of California, Davis
Senior Bridge Engineer, California Department of Transportation

ABSTRACT

This paper discusses portions of a study utilizing the strong motion data obtained from twenty sensors on and near the Painter Street Overcrossing in Rio Dell, California. Particular attention is paid to the influence abutment behavior has on measured response in the three directions of motion of the bridge superstructure. Previous studies have shown that transverse modes of vibration predicted by ambient testing may not reflect behavior during seismic events. The study also focusses on the influence of direction of input boundary motions to be used in analytical models to predict bridge response.

DESCRIPTION OF BRIDGE AND INSTRUMENTATION AND RECORDED DATA

The Painter Street Overcrossing, California bridge number 04-0236, (see Fig. 1) is a continuous two span cast-in-place prestressed post-tensioned concrete box girder bridge located near Rio Dell over Highway 101. The structure has unbalanced spans of 146 and 119 feet and is 52 feet wide. Both end diaphragm abutments and the two-column bent are skewed at 39 degrees. The bent spans 38 feet measured along the centerline of the skewed cross sections and is monolithically connected top and bottom to the footings and superstructure respectively. The columns are approximately 20 feet in height. The abutments have been constructed on top of fill material to provide appropriate vertical clearance over Highway 101 below. The west abutment rests on a neoprene bearing strip which is part of a designed thermal expansion joint. All of the foundations are supported on driven 45 ton concrete friction piles. The bridge is typical of numerous bridges in California spanning two or four lane separated highways.

The Painter Street Overcrossing was instrumented in 1977 by the California Division of Mines and Geology as part of the California Strong Motion Instrumentation Program (CSMIP). The bridge site was instrumented with twenty strong accelerometers capturing various motions on and off the bridge as shown in Fig. 1. Channels 12, 13 and 14 measure free field motions (longitudinal, vertical and transverse to the bridge axis respectively) near the bridge site. At the east end of the bridge, triaxial sets of sensors are located both on the embankment (15, 16, 17) and on the end of the bridge deck (9, 10, 11) so that relative motion between the embankment and the deck could be assessed.

A triaxial set of sensors (1, 2, 3) is also located at the base of the bent's north column to aid in assessing soil-structure interaction. A transverse sensor (7) is located at the base of the deck adjacent to the center bent and vertical sensors are located at midspan of the east (8) and west (6) spans on the north side of the deck. Torsion of the bridge deck cannot be directly assessed since only the north edge of the bridge deck is instrumented.

Since the overpass was instrumented, it has been shaken by six earthquakes starting with the large (6.9ML) Trinidad offshore earthquake of November 8, 1980 at 72 km from the site. The second earthquake was a smaller (4.4ML) event on December 16, 1982 only 15 km from the site. The other events ranged from 5.1 to 5.5 ML at 27 to 61 km. The six earthquakes are summarized in Table 1. Observation of the free field data in Table 1 shows that the maximum vertical accelerations are less than fifty percent of the maximum transverse accelerations and less than

twenty five percent of the maximum longitudinal accelerations. However, the maximum vertical accelerations measured by sensors six and eight on the north end of the deck at the middle of the spans generally equal to or exceed the maximum transverse acceleration measured by sensor 7 of the deck at bent #2. The largest bridge accelerations were caused by caused by the relatively small Rio Dell earthquake of 12/16/82. Unfortunately the free field sensors did not record this event.

TABLE 1 Earthquakes Recorded by Painter Street Instrumentation

Earthquake	Date	Mag. (ML)	Epicent. Distance (km)	Maximum Ground Acceleration C12	C13	C14	Maximum Bridge Acceleration C6	C7	C8
Trinidad	11/08/80	6.9	72	.15g	.03g	.06g	.34g	-	.25g
Rio Del	12/16/82	4.4	15	-	-	-	.39g	.43g	.59g
Cape Mendocino	08/24/83	5.5	61	-	-	-	.27g	.22g	.16g
Event #1	11/21/86	5.1	32	.46g	.08g	.16g	.24g	.26g	.33g
Event #2	11/21/86	5.1	26	.15g	.02g	.12g	.21g	.36g	.29g
Cape Mendocino	07/31/87	5.5	28	.15g	.04g	.09g	-	.34g	.27g

REVIEW OF PREVIOUS WORK

Gates and Smith (1982) performed a comprehensive series of ambient vibration tests on 57 bridges in California in an effort to improve dynamic modeling of bridges. Included in this series of tests were the Meloland Road Overcrossing (Br. No. 58-215) and the Painter Street Overcrossing (Br. No. 4-236). At the time of this study the 1979 Imperial Valley Earthquake had shaken the Meloland Road Overcrossing and it was possible for them to compare natural periods obtained from the ambient vibration tests with the interpretations of the data from the 1979 Imperial Valley Earthquake. They stated "Examination of the results shows that the bridge responds differently to earthquake motions than to ambient vibrations due to the changing soil parameters. It is apparent that even though no inelastic reinforced concrete action took place in the bridge during the earthquake, the abutments experienced the effects of non-linear soil behavior. The abutments acted much looser during the larger excitation of the earthquake than under ambient vibration conditions." They presented the first transverse bridge natural frequency from the ambient results as 3.42 Hz compared to 2.49 Hz from the earthquake result.

Werner, Beck and Levine (1987) studied the strong motion data obtained from the 26 accelerometers installed at the Meloland Road Overcrossing during the 1979 Imperial Valley Earthquake. They used a system identification methodology to assess the seismic response characteristics of the bridge. In their concluding remarks they noted "the abutments and embankments were seen to be the major contributors to the transverse response characteristics of the bridge, whereas the deck structure dominated the MRO's vertical response characteristics." They also presented results indicating modal damping ratios ranging from 0.06 to 0.08 were identified during strong seismic excitation.

Werner, Beck and Nisar (1990) recently presented results comparing the behavior of the Meloland Road Overcrossing during free vibration response following "quick release" tests started from two different initial displacement positions, and the earthquake data from the 1979 Imperial Valley Earthquake. Their data shows significant differences in the transverse response similar to the differences first noted by Gates and Smith (1982). In particular the displacement of the abutments relative to the center of the span is much larger during the real earthquake event and the first transverse natural frequency is much smaller. They also noted a significant increase in the modal damping ratio during the real earthquake compared to the field test program.

Crouse, Hushmand and Martin (1987) performed experimental and analytical studies to determine dynamic soil-structure characteristics of a single-span, prestressed concrete bridge with monolithic abutments supported by spread footings. The experimental program revealed the presence of four modes in the frequency band between 0 to 11 Hz. Three of the modes represented primarily bending and twisting modes of the deck with measured modal damping ratios of 0.020 to 0.035. A fourth mode at 8.2 Hz was primarily in the transverse direction incorporating considerable soil-structure interaction and yielded a measured modal damping ratio of 0.15.

Wilson (1986) studied accelerograms obtained on the San Juan Bautista 156/101 Separation Bridge during the 6 August 1979 Coyote Lake earthquake. The bridge consists of six spans with the abutments and bents skewed at 34.8° with respect to the bridge deck. The main shock produced a magnitude $M_L = 5.9$ with a maximum ground acceleration of 0.12g at an epicentral distance of 26km. To model the actual field behavior of the bridge it was necessary to place a linear translational spring in the longitudinal direction of the bridge. One significant conclusion of the study showed that the modal damping ratio for the dominantly longitudinal fundamental mode approximately doubled during the strong motion phase from 4 to 8 seconds compared to the initial value of 5.4 percent. At low levels of vibration it was inferred one might reasonably expect 3 to 6 percent damping in the fundamental mode. This indicates certain energy dissipation mechanisms are activated at higher levels of response. Damping in the second horizontal mode ranged from 7.3 to 13.4 percent during five time segments of the record evaluated.

Maroney, Romstad and Chajes (1990) presented results from data obtained during six different earthquake events at the instrumented Painter Street Overcrossing. It was only possible to capture the actual measured natural frequencies and superstructure accelerations by using a relatively soft transverse spring at each abutment. Fixing the abutments resulted in a computed first transverse natural period of 0.16 seconds compared to the measured transverse period of 0.28 seconds. The results of that study indicating the importance of appropriately modeling the abutment served as the motivation for this study.

OBSERVED BEHAVIOR OF PAINTER STREET OVERCROSSING

Table 2 presents the complete set of maximum accelerations from all sensors for earthquakes 4, 5 and 6 arranged by direction. These are simply listed here because they contain essentially complete data sets including free field and sensor 7. In each direction the free field motion is given first followed by the base of pier motion. The remaining channels are then listed in sequential order from the west abutment fill to east abutment fill.

TABLE 2. Maximum Accelerations from Earthquakes 4, 5 and 6

	Longitudinal Max. Accel. (g/100)					Transverse Max. Accel. (g/100)							Vertical Max. Accel. (g/100)							
	Channel					Channel							Channel							
Earthquake	12	1	18	11	15	14	3	20	4	7	9	17	13	2	19	5	6	8	10	16
11/21/86*	46	27	45	40	40	16	13	30	23	26	23	23	8	8	18	10	23	33	25	11
11/21/86**	15	11	17	19	17	12	12	25	25	35	30	22	2	5	6	5	20	29	14	4
07/31/87	15	11	20	21	17	9	10	17	18	34	25	26	4	6	19	5	-	26	11	5

Longitudinal Motion

It is interesting to note the maximum longitudinal accelerations on the abutment fill (15 and 18) and on the structure (11) are essentially the same as the free field motion (12) for all earthquakes. This may indicate the bridge is moving as a rigid body with the ground in the longitudinal direction. Figure 2 presents the Fourier Amplitude Spectra for the longitudinal free field motions and the longitudinal sensor on the fill at the east abutment. Although the frequency content is somewhat smoother on the fill, there is no general amplification through a broad frequency range. This spectra is representative of the other earthquake records for the longitudinal motions. Fourier

Spectra at sensors 11 and 15 are generally very similar. Surprisingly, the longitudinal motion at the base of the pier (3) is consistently attenuated relative to all other longitudinal motion.

Vertical Motion

All vertical sensors on the fill (16 and 19) and bridge (5, 6, 8 and 10) are amplified relative to the free field (13) and base of pier (2) except sensor 5 on the west bridge abutment. This is probably due to the bearing strip which exists at the base of this abutment. This influence is rather dramatically demonstrated by viewing the acceleration response spectra for the vertical sensor 19 on the fill and sensor 5 adjacent to it, but on the bridge, shown in Figure 3. The motion is attenuated for all periods less than 0.33 seconds. The opposite effect can be seen by viewing Figure 4 showing the same two spectra for vertical sensor 16 on the fill and vertical sensor 10 on the bridge at the east abutment. At this abutment the vertical motion is generally amplified on the bridge abutment relative to the fill.

Transverse Motion

In the transverse direction, Table 2 shows all sensors on the abutment fill (17 and 20) and on the structure (4, 7 and 9) are considerably amplified relative to the free field (14) and base of pier motion (3). Figure 5 shows average Fourier Amplitude Spectra for all recorded transverse free field motions, base of pier motions, and on the fill and on the bridge abutment at the east end. The free field and base of pier motions are similar indicating very little soil-structure interaction. However, the motion in the free field, on the abutment fill and on the bridge abutment are significantly different in dicating relative motion between all three locations. This has considerable implication for analytical modeling.

Transverse motions are also quite different at the two abutments because of the difference in the construction of the two abutments. The influence of the bearing strip and shear keys at the west abutment can be seen in Figure 6 by observing the transverse time history of acceleration motions as the waves arrive first at the west abutment, then the free field station and then the east abutment. Inspecting sensor 4 on the abutment above the bearing strip and shear key shows very eratic motion with the arrival of the first strong wave. Similar behavior can be observed at sensor 4 in every recorded motion. In some instances the acceleration appears to hold relatively constant, indicating either sliding or plastic resistance in the abutment, and in other instances dramatic reversals in direction occur indicating impacting has occurred.

ABUTMENT BOUNDARY CONDITIONS

The interpretation of recorded data at other bridge sites and this brief description of the recorded data at Painter Street indicates the actual load-deformation behavior of the Painter Street abutment system is extremely complicated to model due to factors such as the

1) interaction of soil, piles, footings, shear keys, abutment backwall, abutment wingwalls, bearing strip,
2) nonlinearities due primarily soil stress-strain characteristics, opening and closing of gaps (impacts), friction surfaces,
3) time effects such as long term prestress shortening, thermal state relative to original thermal state, lockup of gaps caused by foreign materials,
4) coupling of longitudinal and transverse motion due to skew effects,
5) "effective mass" of the wingwall/backfill system, and
6) material, frictional and radiation damping.

Stiffness resistance to deformation at the abutments may be described by a complex system of springs reflecting soil, pile, concrete and interaction properties. Figures 7 and 8 shows plan and elevation views of the abutment system with schematic springs attached approximating resistance of individual elements to longitudinal motion (global X) of the bridge deck. Similar models have been constructed for transverse (global Z) and vertical (global Y) resistance.

At both abutments the "simple beam" wingwalls are not monolithically connected to the abutment backwall or its foundation. Over the height of the wingwalls an effectively pinned connection exists with respect to moment about the vertical global Y axis. The transfer of shear from the

backwall to the wingwalls in the transverse global Z direction is one directional in that resistance the movement of the wing wall out from the centerline of the bridge is resisted once the joint filler is crushed to transfer the load. However, the connection offers no resistance to movement of the wingwall toward the longitudinal centerline of the bridge except frictional resistance at the base of the wingwall where it rests on the abutment backwall footing. At this location the wingwalls and abutment backwall footing are separated by 1/4" of expansion joint filler. The same pinned joint interrupts the transfer of load to the wingwalls and back to the rear piles in the longitudinal global X direction until one inch of expansion joint filler is sufficiently crushed. Once the joint filler is sufficiently compressed resistance forces between the wingwalls, rear pile caps, rear piles and soil can be developed when the deck is moving into the backfill material.

At the base of the west abutment there is not a monolithic connection between the abutment backwall and the abutment footing. The backwall and the foundation are separated by a 1/4" neoprene bearing strip. Shear keys effectively bound the abutment backwall in the case of gross relative displacements in both transverse directions and in the skewed longitudinal direction such that the backwall is keyed against moving into the soil. The abutment backwall and the transverse shear keys are separated by one inch of expansion joint filler. In the skewed longitudinal direction the abutment backwall and the shear key at the time of construction were separated by one inch of expansion joint filler; however the separation at any time since the original construction is a function of the time effects noted. Friction and shear stiffness of the bearing strip offer the only load path to the footing from the abutment backwall prior to the expansion joint filler being compressed sufficiently to transfer compressive stresses.

A 39 degree skew at both abutments forces the normal and shear abutment resistance to be defined at an angle to the global axes. Movement of the abutment backwall into the abutment backfill in the global X direction is resisted by passive soil forces normal to the abutment backwall and frictional forces parallel to the abutment backwall which have components in the global X and Z directions.

Figure 9 presents an articulated set of longitudinal components of the springs in series and in parallel at west abutment where the bearing strip is located. The springs can be combined to represent a single nonlinear spring in the longitudinal direction. Similar models have constructed for the global Y and Z directions. The complete assembled set can be combined to form a coupled set of six degree of freedom nonlinear springs at a point on the abutment backwall if a stick model is employed, or a coupled set of distributed nonlinear springs at nodal points along the abutment backwall if the deck is modeled as a plate system. Due to space limitations herein only the longitudinal springs at the west abutment will be described.

Conceptually we will describe the mechanisms by thinking of the bridge deck moving into, or away, from the backfill material. A portion of the deck load will transfer through the stiffness K_{bw} of the abutment backwall above the abutment footing to the bearing strip of stiffness K_{bs}. Initially this portion of the deck load will then be transferred into the soil through the piles, K_p, and passive resistance against the cap, K_{cf}, and through the friction where the wingwall rests on the cap, $K_{ww/cf}$. The portion of the deck load not transferred to the footing from the backwall will directly transfer from the backwall to the soil through $K_{bw/s}$ representing the distributed resistance of the entire backwall area about the abutment footing. This stiffness is represented by the relatively confined soil behind the abutment backwall and the unconfined soil on the roadway side of the wall.

The load transferred to the wingwall will be distributed to the surrounding soil medium through cohesion and frictional resistance of the soil confined between the wingwalls, $K_{ww/si}$, and unconfined outside the wingwalls, $K_{ww/so}$, the horizontal component, K_{wwl}, of the normal and frictional resistance of the thickness at the base of the wingwall, the resistance of the soil to the thickness of the wingwall above the rear footing, K_{wwu}, the passive resistance to the cap, K_{cr}, and the piles, K_p, at the rear footing for the wingwalls.

Discontinuities or "gaps" at the abutment backwall/wingwall connection, D_{ww}, and abutment backwall/pilecap connection, D_{cf}, are also identified in Figure 9. The displacement D_{ww} is the deformation of the backwall required to engage the wingwall directly and D_{cf} is the deformation of the base of the backwall required to engage the pilecap directly through its shear key. Closure and opening of these gaps will result in major instantaneous stiffness discontinuities which should be observable in the recorded data.

INFLUENCE OF THREE DIRECTIONS OF MOTION ON PREDICTED RESPONSE

Elastic response spectra and time history analysis of the Painter Street Overcrossing have been carried out as part of this study using all three direction of ground motion. The comparisons of the measured results and the predicted results are only fair at this point, and space prohibits showing many of the comparisons. The clear nonlinear behavior in the abutment region and substantial differences in damping between modes makes elastic analysis almost a qualitative comparison. Table 3 is presented to demonstrate the significance both the vertical and transverse free field motions have on the accelerations at stations 6, 7 and 8. Clearly both directions of motion contribute significantly to the vertical accelerations 6 and 8 on the north edge of the deck at the middle of each of the spans. As expected, the transverse acceleration at the bent is dominantly contributed by the transverse input motion.

Table 3 Maximum Response Spectrum Predictions of Superstructure Accelerations

Earthquake	Free Field Input Direction	Center West Span (ft/sec^2) Vertical Acc 6	Center East Span (ft/sec^2) Vertical Acc 8	Center Bent Span (ft/sec^2) Transverse Acc 7
4	Vertical (13)	6.7	9.2	1.3
	Longitudinal (12)	0.3	0.4	0.0
	Transverse (14)	9.2	7.6	12.6
5	Vertical (13)	2.2	2.4	0.5
	Longitudinal (12)	0.0	0.0	0.0
	Transverse (14)	8.5	6.8	12.1
6	Vertical (13)	3.5	4.1	0.8
	Longitudinal (12)	0.0	0.0	0.0
	Transverse (14)	7.8	5.9	11.2

SUMMARY AND CONCLUSIONS

Relatively short span bridges exhibit considerable soil-structure interaction in the abutment area due to nonlinear soil behavior, gaps in abutment construction, bearing strips. It appears the phenomenon cannot be observed by ambient and quick release field testing. Damping varies significantly between modes depending upon the level of soil-structure interaction present in the mode. Elastic modeling is unlikely to provide other than qualitative information on the peak forces in bridges dominated by soil struction interaction in the abutment area.

ACKNOWLEDGEMENTS

The contents of this report were developed under a contract from the California Department of Conservation, Division of Mines and Geology, Strong Motion Instrumentation Program. However, these contents do not necessarily represent the policy of that agency nor endorsement by the State Government. The authors greatly appreciative the support of the California Department of Transportation, Office of Structures, for the use of the computer time and facilities in conducting this study.

REFERENCES

Chen, M. and Penzien, J., "Nonlinear Soil-Structure Interaction of Skew Highway Bridges," Report No. UCB/EERC-77/24, Earthquake Engineering Research Center, University of California, Berkeley, August, 1977.

Crouse, C. B., Hushmand, B., and Martin, G. R., "Dynamic Soil-Structure of a Single Span Bridge", Earthquake Engineering and Structural Dynamics, Vol. 15, 1987, pp. 711-729 .

Douglas, B.M., Maragakis, E.A., Vrontinos, S. and Douglas, B.J., "Analytical Studies of the Static and Dynamic Response of the Meloland Road Overcrossing," Proceedings of the Fourth U.S. National Conference on Earthquake Engineering, Palm Springs, Ca., Vol. 1, 1990, pp. 987-996.

Gates, J.H. and Smith, M.J., "Verification of Dynamic Modeling Methods by Prototype Excitation," Report No. FHWA/CA/SD-82/07, California Department of Transportation, Office of Structures Design, Sacramento, Ca., November, 1982.

Lam, I. and Martin, G., "Seismic Design of Highway Bridge Foundations", FHWA/RD-86/101, Earth Technology Corporation, Long Beach, Ca., June 1986.

Levine, M.B. and Scott, R.F., "Dynamic Response Verification of a Simplified Bridge-Foundation Foundation Model," ASCE, Journal of Geotechnical Engineering, Vol. 115, No. 2, February, 1989, pp. 246-260.

Maragakis, E., "A Model for the Rigid Body Motions of Skew Bridges," Report No. EERL 85-02, California Institute of Technology, 1985.

Maragakis, E., Thornton, G., Saiidi, M. and Siddharthan, R., "A Simple Non-Linear Model for the Investigation of the Effects of the Gap Closure at the Abutment Joints of Short Bridges," Earthquake Engineering and Structural Dynamics, Vol. 18, 1987, pp. 1163-1178.

Maroney, B., Romstad, K.M. and Chajes, M.J., "Interpretation of Rio Dell Freeway Response During Six Recorded Earthquake Events," Proceedings of the Fourth U.S. National Conference on Earthquake Engineering, Palm Springs, Ca., Vol. 1, 1990, pp. 1007-1016.

Werner, S.D., Beck, J.L. and Levine, M.B., "Seismic Response Evaluation of Meloland Road Overpass Using 1979 Imperial Valley Earthquake Records," Earthquake Engineering and Structural Dynamics, Vol. 15, 1987, pp. 249-274.

Werner, S.D., Beck, J.L. and Nisar, A., "Dynamic Tests and Seismic Excitation of a Bridge Structure," Proceedings of the Fourth U.S. National Conference on Earthquake Engineering, Palm Springs, Ca., Vol. 1, 1990, pp. 1037-1046.

Wilson, J. C., "Analysis of the Observed Seismic Response of a Highway Bridge," Earthquake Engineering and Structural Dynamics, Vol. 14, 1986, pp. 339-354.

Wilson, J. C., "Stiffness of Non-Skew Monolithic Bridge Abutments for Seismic Analysis", Earthquake Engineering and Structural Dynamics, Vol. 16, 1988, pp. 867-883.

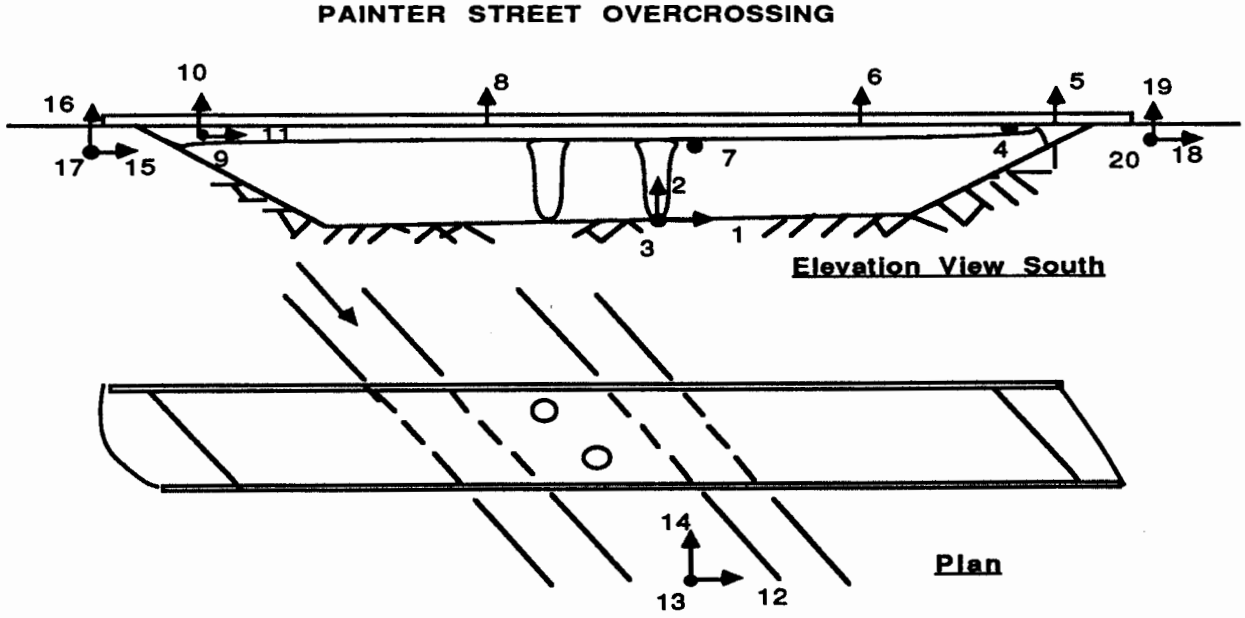

Figure 1 Superstructure and Instrumentation for Painter Street Overcrossing

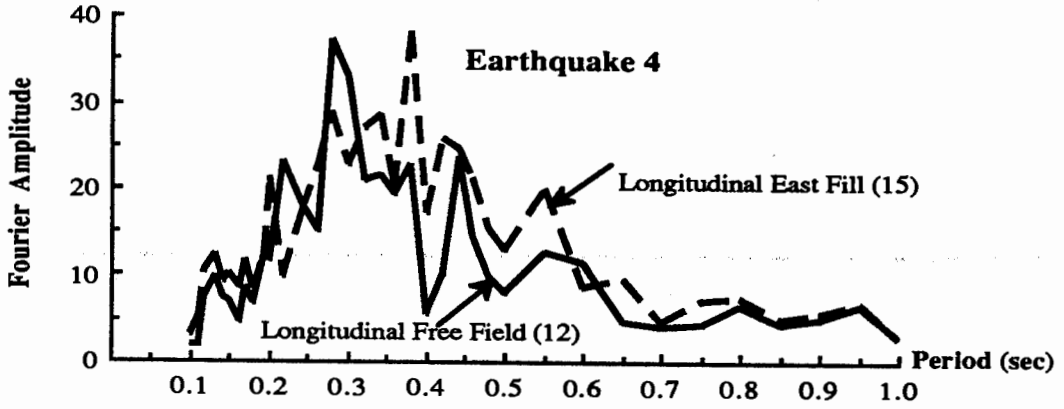

Figure 2 Fourier Amplitude for Longitudinal Motion at Sensors 12 and 15

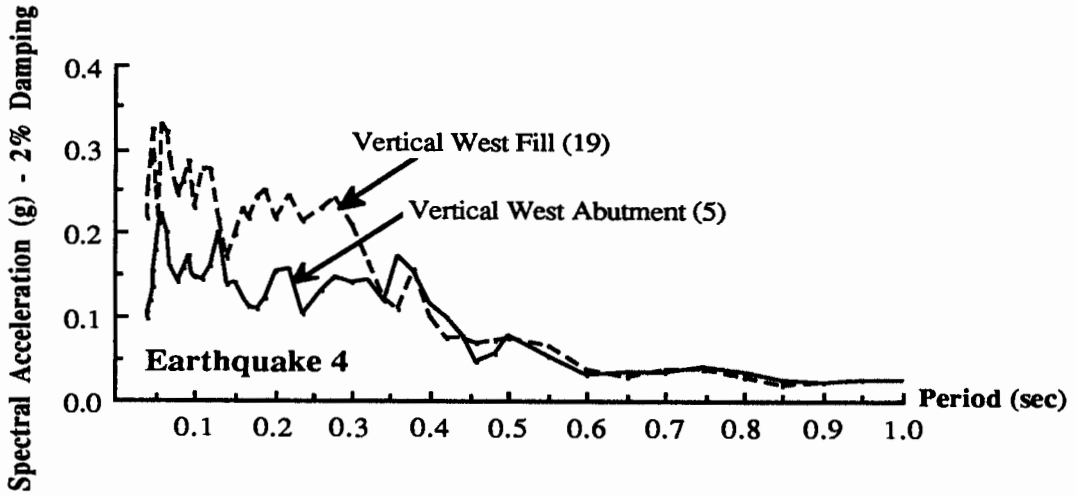

Figure 3 Acceleration Spectra for Vertical Sensors 5 and 19 at West Abutment

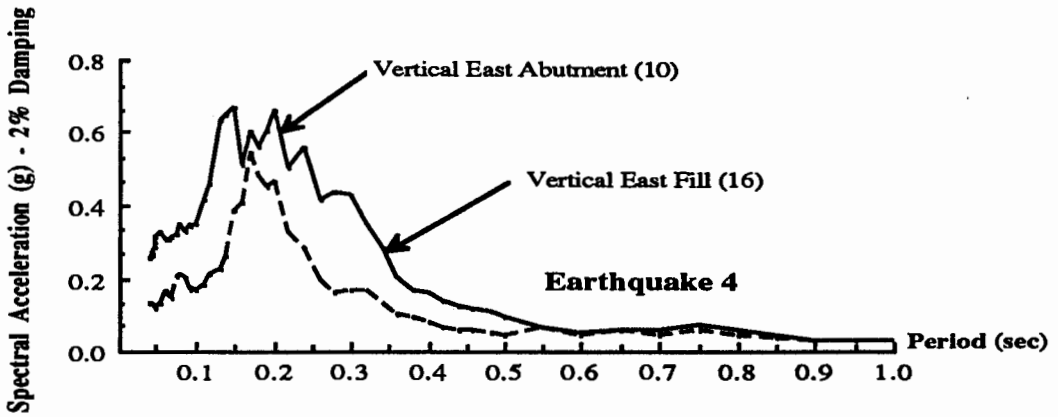

Figure 4 Acceleration Spectra for Vertical Sensors 10 and 16 at East Abutment

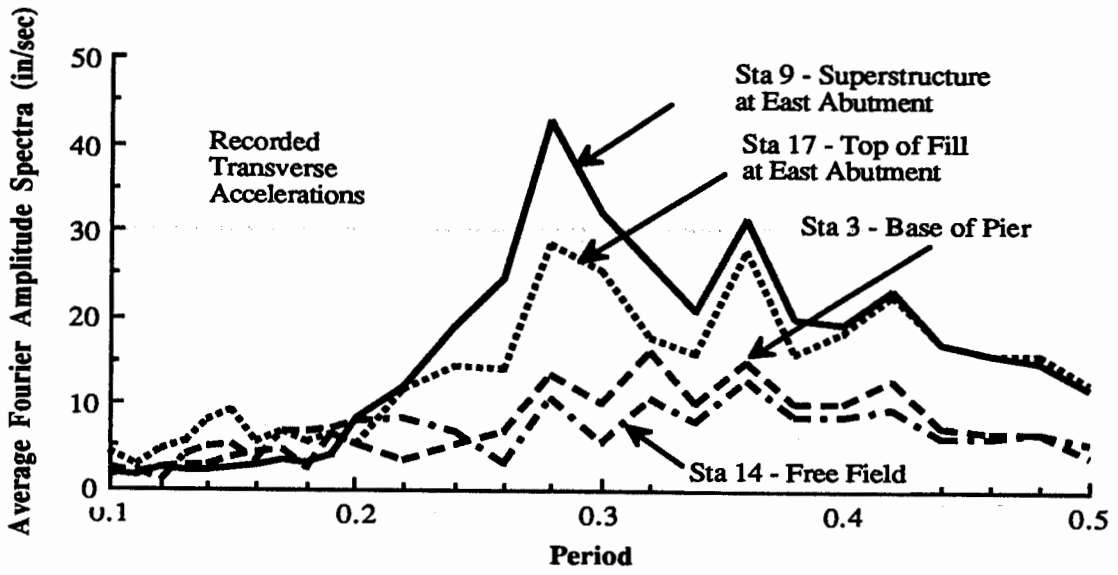

Figure 5 Average Fourier Amplitude Spectra for All Recorded Motions at 14, 3,17 and 9

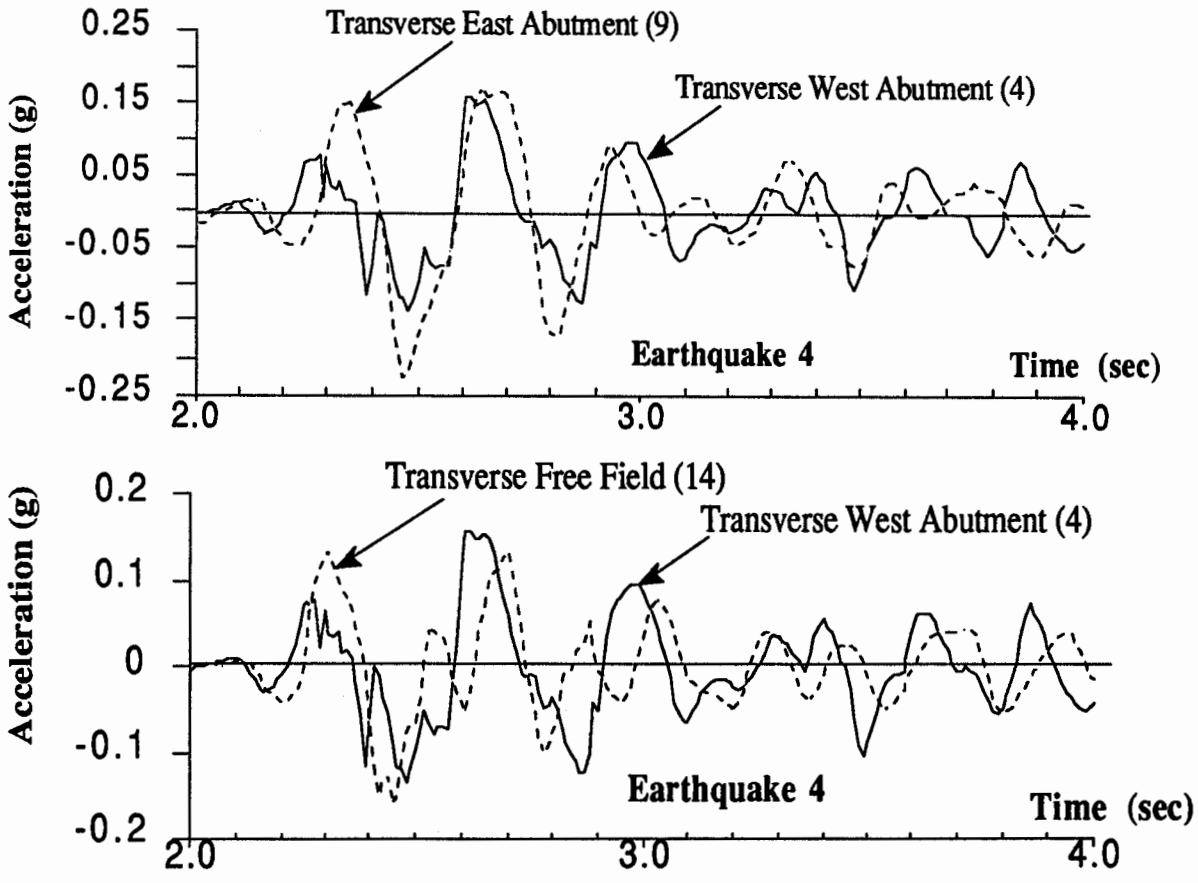

Figure 6 Recorded Transverse Time History Motions at 4, 9 and 14 During Earthquake 4

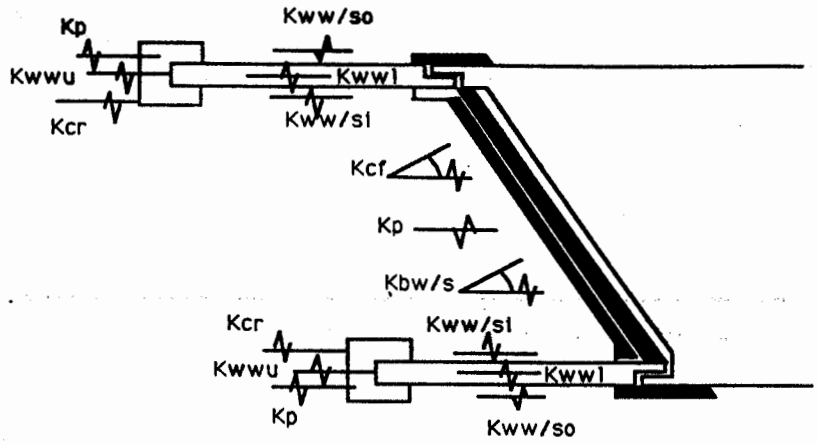

Figure 7 Plan View of Longitudinal West Abutment Resisting Elements

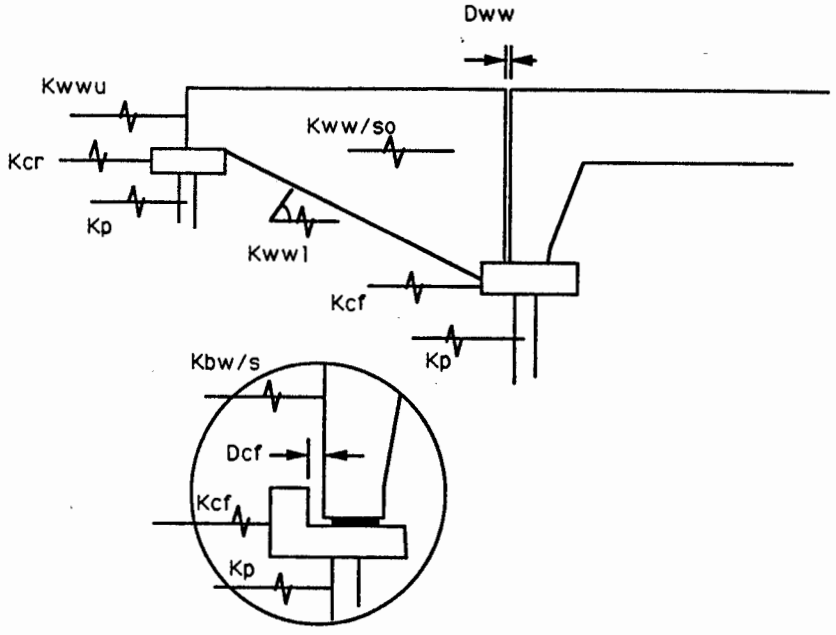

Figure 8 Elevation View of Longitudinal West Abutment Resisting Elements

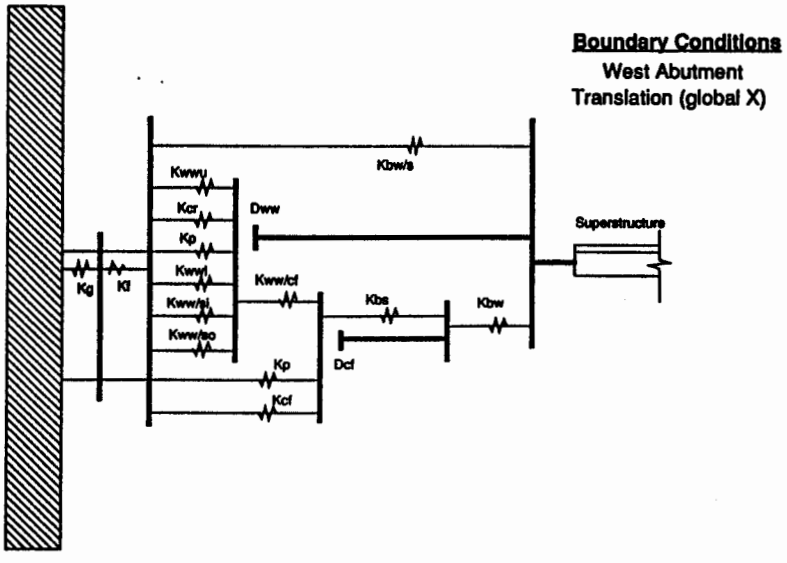

Figure 9 Schematic Representation of Longitudinal West Abutment Active Spring Elements